1   **The large mean body size of mammalian herbivores explains the**

2   **productivity paradox during the last glacial maximum**

3   **Dan Zhu[1*], Philippe Ciais[1], Jinfeng Chang[1,2], Gerhard Krinner[3], Shushi Peng[4], Nicolas**

4   **Viovy[1], Josep Peñuelas[5], Sergey Zimov[6]**

5   [1] Laboratoire des Sciences du Climat et de l'Environnement, LSCE CEA CNRS UVSQ,
6   91191 Gif Sur Yvette, France

7   [2] Sorbonne Universités (UPMC), CNRS-IRD-MNHN, LOCEAN/IPSL, 4 place Jussieu,
8   75005 Paris, France

9   [3] CNRS, Univ. Grenoble Alpes, Institut de Géosciences de l'Environnement (IGE), Grenoble,
10 France

11 [4] Sino-French Institute for Earth System Science, College of Urban and Environmental
12 Sciences, Peking University, Beijing 100871, China

13 [5] CSIC, Global Ecology Unit, CREAF-CSIC, Universitat Autònoma de Barcelona, Bellaterra,
14 08193 Catalonia, Spain

15 [6] Northeast Science Station, Pacific Institute for Geography, Russian Academy of Sciences,
16 Cherskii 678830, Russia

17

18 Corresponding author: Dan Zhu (dan.zhu@lsce.ipsl.fr)

19

20 **Abstract**

21 Large herbivores are a major agent in ecosystems, influencing vegetation structure and carbon
22 and nutrient flows. During the last glacial period, the steppe-tundra ecosystem prevailed on
23 the unglaciated northern lands, hosting a high diversity and density of megafaunal herbivores.
24 The apparent discrepancy between abundant megafauna and the expected low vegetation
25 productivity under a generally harsher climate with lower CO_2 concentration, termed
26 productivity paradox, awaits large-scale quantitative analysis from process-based ecosystem
27 models. Yet most of the current global dynamic vegetation models (DGVMs) lack explicit
28 representation of large herbivores. Here we incorporated a grazing module in the
29 ORCHIDEE-MICT DGVM based on physiological and demographic equations for wild large
30 grazers, taking into account feedbacks of large grazers on vegetation. The model was applied
31 globally for present-day and the last glacial maximum (LGM). The present-day results of
32 potential grazer biomass, combined with an empirical land use map, infer a reduction of wild
33 grazer biomass by 79-93% due to anthropogenic land replacement over natural grasslands.
34 For the LGM, we find that the larger mean body size of mammalian herbivores than today is
35 the crucial clue to explain the productivity paradox, due to a more efficient exploitation of
36 grass production by grazers with a larger-body size.
37

38   Mammalian herbivores live in major terrestrial ecosystems on Earth[1]. During the past decades,

39   our understanding has increased about the important role of large mammalian herbivores

40   (body mass >10 kg)[2] in controlling vegetation structure and carbon and nutrient flows within

41   ecosystems. In herbivore-exclusion experiments, large herbivores have been shown to reduce

42   woody cover[3,4], modify the traits and composition of herbaceous species[5,6], accelerate nutrient

43   cycling rates[7,8], increase grassland primary production[9,10], and reduce fire occurrence[11]. In

44   paleo-ecological studies, the late Pleistocene megafaunal extinctions have been shown to

45   result in cascading effects on vegetation structure and ecosystem function[12], including biome

46   shifts from mixed open woodlands to more uniform, closed forests, and increased fire

47   activities[13,14].

48   During the last glacial period from 110 to 14 ka BP (before present), the mammoth steppe

49   ecosystem, also referred to as "steppe-tundra" or "tundra-steppe"[15], prevailed in Eurasia and

50   North America, covering vast areas that are occupied by boreal forests and tundra today[16–20].

51   Characterized by a continental climate, intense aridity, and domination of herbaceous

52   vegetation including graminoids, forbs and sedges, the mammoth steppe sustained a high

53   diversity and probably a high density of megafaunal herbivores like woolly mammoth,

54   muskox, horses, and bison[19,21–23]. Yet the main driving force of the maintenance and

55   disappearance of mammoth steppe remains controversial. Alternative to the climate

56   hypothesis which attributes the end-Pleistocene vegetation transformation and mammalian

57   extinctions to climate change, the "keystone herbivore" hypothesis argues that

58   megaherbivores have maintained mammoth steppe through complex interactions with

59   vegetation, soil and climate[18,24,25].

60   The apparent discrepancy between the late Pleistocene dry and cold climates and the abundant

61   herbivorous fossil fauna found in the mammoth steppe biome has provoked long-standing

62   debates, termed as "productivity paradox" by some paleontologists[26]. Through the general

63   relationship that larger animals require less food per unit body weight, Redmann[27] indicated

64   that higher herbivore biomass densities could be maintained if large species dominate the

65   ungulate community. Studies of modern analogous steppe communities in north-eastern

66   Siberia emphasized the mosaic character of vegetation as a crucial factor in supporting

67   herbivores, with various herbaceous plant types and landscape units of different productivities,

68   depending on local heat and moisture supply affected by local topography[15,21]. However, a

69   large-scale quantitative analysis is missing about how local evidences for abundant

70   megafauna[19,23] can be reconciled with low vegetation productivity under glacial climates and

71   low atmospheric CO_2 concentrations[28], calling for the integration of interactions between

72   large herbivores and terrestrial productivity within process-based ecosystem models.

73   Over the past 20 years, dynamic global vegetation models (DGVMs) have been developed

74   and applied to simulate the global distribution of vegetation types, biogeochemical cycles, and

75   responses of ecosystems to climate change[29]. However, despite the non-negligible ecological

76   impacts of large herbivores, most of the current DGVMs, or land surface models that include

77   a dynamic vegetation module, lack explicit representation of large herbivores and their

78   interactions with vegetation. One exception is the LPJ-GUESS which included a grazer

79   module[30] and was applied to present-day Africa to study the potential impact of large grazers

80   on African vegetation and fire[31].

81   In this study, aiming to address the productivity paradox, we extended the modelling domain

82   to the globe for two distinct periods, present-day and the last glacial maximum (LGM, ca. 21

83   ka BP), using the ORCHIDEE-MICT DGVM model[32,33]. We incorporated the dynamics of

84   large grazers within ORCHIDEE-MICT based on equations describing grass forage intake

85   and metabolic rates dependent on body size, and demographic parameters describing the

86   reproduction and mortality rates of large grazers[30,34] (Fig. 1). Feedbacks of large grazers on

87   vegetation were simulated through simplified parameterizations for trampling of trees, grass

88   biomass removal, and productivity enhancement by grazing calibrated from field experiments

89   (Fig. 1, see detailed description in Methods section "Effects of grazers on vegetation").

90   Grazers were represented with a prescribed average body size, while browsers (i.e. herbivores

91   feeding on woody plants) were not included, assuming herbaceous plants to dominate the diet

92   of large herbivores[17,35,36]. Simulated present-day grazer biomass were evaluated against field

93   observations in protected areas across a wide range of ecosystems. For the LGM, we found

94   that the larger mean body size of grazers than today is the key parameter that allows the

95   model to reproduce a substantial density of large grazers on the cold steppe during the LGM.

96

97

Results

Present-day grazer biomass

Simulated grazer biomass densities are shown in Fig. 2 for present-day (PD) climate conditions. They were in reasonable agreement with the herbivore densities observed in protected areas from Hatton et al.[37] (Fig. 2b). Model-data misfits may be due to simplifications of the grazing module (see Methods). First, the lack of browsing process underestimates food availability for herbivores. This leads to an underestimate for large herbivore populations not only because of missing browsers and underestimated mixed feeders, but also because of underestimated grazers, since conventional grazers can have some portion of woody plants as well in their diets, affected by available forage types[35,36]. Second, the lack of explicit representation of predation, competition for resources like water and shelter, poaching in protected areas, outbreak of diseases[38], and hunting in the North American ecosystems[39], may lead to an overestimation of large grazer biomass compared to the Hatton et al.[37] data. In addition, bias of grass productivity in the model can also result in errors in the modelled grazer density. We verified that the simulated global pattern of grass gross primary productivity (GPP) generally matches an observation-driven dataset[40], yet with an overestimation in subarctic regions (Supplementary Fig. 1). This overestimation of grass GPP might be due to the high grass fractional cover produced by the vegetation dynamics module (Supplementary Fig. 1a) which does not represent shrubs, mosses and lichens[33].

Figure 2a shows the modelled global distribution of potential grazer biomass density for PD, after subtracting the fractions of tropical rainforest (see Supplementary Note 1). In order to estimate the reduction of wild large grazers due to human land use, we made use of the anthropogenic biome classification system from the Anthromes version 2 product[41], which separated three major categories: *Used*, *Seminatural*, and *Wild*. We assumed the remnant habitat for large grazers to be the *Wild* category as a lower estimate, and the *Seminatural* and *Wild* categories as an upper estimate. The resulting spatial distributions are shown in Supplementary Fig. 2, and the regional total values are listed in Supplementary Table 2.

Simulated global potential biomass of large grazers for PD was slightly smaller than the pre-industrial (PI) value (Supplementary Table 2), mainly due to a slight decrease in modelled grassland area. This indicates that climate change and the increase of CO_2 by 100 ppm during the past century have had minor effects on potential grazer biomass. However, subtracting the used land by humans led to a 41-83% reduction of the potential biomass of wild grazers for PI,

4

130 and an even greater reduction (79-93%) for PD due to the expansion of agricultural land use
131 and settlements during the past century. Note that the estimated reduction here only considers
132 the direct replacement of wildlife habitats by human land use, whereas other threats to wild
133 grazers including hunting, competition with livestock, disease transmission from domestic to
134 wild species, loss of genetic diversity, and the synergies among these threats[42], are not
135 included.

136 **LGM grazer biomass**

137 The biomass of large grazers at the LGM is closely related to the vegetation distribution and
138 its productivity. In order to evaluate the simulated LGM vegetation, the plant functional types
139 of the model were regrouped into the mega-biomes of the BIOME 6000 reconstruction based
140 on pollen and plant macrofossil data[43] (Supplementary Note 2). The model can capture the
141 retreat of forests in the northern middle and high latitudes during the LGM, largely replaced
142 by grassland and tundra, in accordance with BIOME 6000 data (Fig. 3a and 3b). The scarcity
143 of palaeoecological records, however, precludes a more quantitative evaluation of the
144 modelled vegetation distribution.

145 Figure 3c shows the simulated LGM grazer biomass density for the Northern Hemisphere.
146 The spatial distribution can generally match the distribution of megafaunal fossil occurrences,
147 with 60% of the locations where fossils have been found being in grid cells with a grazer
148 density larger than 500 kg km^{-2} (Fig. 3c). Compared with two reconstructions of large
149 herbivore density of ca. 9 tonne km^{-2} by Zimov et al.[19] in northern Siberia and by Mann et
150 al.[23] in arctic Alaska averaged for the period of 40-10 ka BP, our simulated grazer density was
151 only ca. 1 tonne km^{-2}. This large underestimation is possibly due to: 1) a low bias of our
152 model results using LGM climate, since the reported bone abundance is an average during 40-
153 10 ka BP[19,23], a period during which LGM corresponds to the most severe climate, 2)
154 uncertainties in the LGM climate used to force our DGVM model, considering limitations of
155 climate models in capturing sub-continental patterns of temperature and precipitation for the
156 LGM[44]; and 3) the coarse resolution (ca. 30,000 km^2 for one pixel near 70°N) of our model
157 results that do not capture local conditions of the areas from where densities were
158 reconstructed (river banks and lowland sections of 10-80 kilometers[19,23]). A simple sensitivity
159 test was conducted for the two grid cells corresponding to the studies of Zimov et al.[19] and
160 Mann et al.[23], by setting temperature to be warmer by 1 or 2°C and annual rainfall to be
161 higher by 50% or 100% (Supplementary Fig. 3). Grazer biomass density for both grid cells

162   could increase to 4 tonne km^{-2} in the case of +2°C warmer temperature and 100% higher

163   rainfall, indicating a strong sensitivity of grazer biomass to the slightly milder climates in the

164   context of very cold and dry conditions. This strong sensitivity is supported by the evidence

165   of high variations in megafaunal populations during 45-10 ka BP, with peaks of bone

166   abundance at warm interstadial periods[45].

167   **Effects of temperature and body size on grazer biomass density**

168   Climate conditions control large grazer densities through grass NPP supporting herbivores

169   and the herbivore-ecosystem feedbacks (see Fig. 1). For present-day Africa, modelled

170   relationship between potential grazer density and mean annual precipitation (MAP) was

171   unimodal (Fig. 4a, red), close to the relationship found by ref[46] based on observations (Fig. 4a,

172   grey). The grazer density showed a peak at ca. 700 mm MAP, and gradually decreases under

173   higher MAPs mainly due to grasslands being out-competed by trees, despite trampling by

174   herbivores. This unimodal relationship mirrors the relationship between modelled grass NPP

175   and MAP (Fig. 4a, blue), because of the roughly linear relationship between potential grazer

176   density and grass NPP in Africa (Fig. 4a, green).

177   For the globe, however, the relationship between grass NPP and potential grazer density was

178   strongly affected by mean annual temperature (MAT) (Supplementary Fig. 5). In regions with

179   MAT above ca. 0 °C, the grazer biomass-to-grass NPP ratio generally stayed in the range 5-

180   10 (in kg live weight km^{-2} : g C m^{-2} yr^{-1}) (Fig. 4b); whereas in colder regions, the same grass

181   productivity supported much less grazers, with barely any grazers when MAT is below -10 °C.

182   This strong reduction of grazer biomass per unit of grass NPP under low MATs resulted from:

183   1) the energy expenditure which increases exponentially with decreasing temperature for

184   mammals (Methods equation (3)), and 2) the growing season being shorter in high latitude

185   regions compared to tropical and temperate regions, which leads to longer starvation period

186   with low temperatures, acting to reduce fat reserves and birth rates and to increase starvation-

187   induced mortality (Methods equations (6)-(8)).

188   Body size is a key parameter in the physiological equations in the model (see Methods). In the

189   LGM run with body size (A) prescribed as 500 kg ind.$^{-1}$ (per individual), derived from the

190   reconstructions by Mann et al.[23] and Zimov et al.[19] based on the relative bone abundance of

191   different taxa, the grazer biomass-to-grass NPP ratios were higher than in the PD run,

192   especially for colder regions (Fig. 4c red). The strong reduction of this ratio occurred only

193   below an MAT threshold of ca. -10 °C, instead of 0 °C in the PD run. We further conducted a

194 sensitivity test for the same LGM run except that A was prescribed as 180 kg ind.[-1], the same

195 as for PD in the northern hemisphere[37] (see Methods). The relationship between the grazer

196 biomass-to-grass NPP ratio and MAT (Fig. 4c blue) was broadly similar to that in the PD run,

197 despite larger variations than PD for MATs near 5 °C. Thus, Fig. 4c shows that a larger body

198 size in the LGM effectively counteracted the effect of colder temperatures on grazer density.

199 As denoted in Methods equations (1) and (3), when body size increases, the maximum forage

200 intake rate increases faster than the energy expenditure, because the scaling exponent of

201 intake in equation (1) (0.88 for grass living biomass and 0.84 for dead grass) is larger than

202 that of energy expenditure (0.75). This leads to a more efficient exploitation of grass

203 production by grazers with a larger-body size, thus a higher grazer density supported by the

204 same level of grass production.

205 The spatial distribution of grazer biomass at the LGM in the sensitivity test with A equalling

206 to 180 kg ind.[-1] is presented in Supplementary Fig. 6, showing that grazers could have barely

207 existed in the mammoth steppe ecosystem in Eurasia and North America if they had a body

208 mass as low as today's northern herbivores. The global total grazer biomass would be only

209 235 million tonnes live weight, much less than that with A equalling to 500 kg ind.[-1] (319

210 million tonnes). This suggests that, during the LGM, the cold steppe in the middle and high

211 latitudes was able to sustain substantial quantities of grazers mainly because the mean grazer

212 body size was much bigger than today.

213 **Impacts of grazing on land carbon cycle during the LGM**

214 Due to the strong human intervention in today's biosphere[47] and the human-caused collapse

215 of large herbivore populations[42], we focus on the LGM to analyse the impacts of grazing on

216 vegetation distribution and the carbon cycle, by comparing the model results with and without

217 grazers. Figure 6 presents the effect of grazers on the global land carbon fluxes during the

218 LGM. Total NPP simulated with grazers was 35 Pg C yr^{-1}, 17% higher than without grazers.

219 Turnover times of tree and grass biomass decreased from 12.5 and 0.57 years without grazers

220 to 11.8 and 0.52 years with grazers. For trees, the additional trampling-induced mortality

221 contributes to the faster turnover rate and lower equilibrium biomass than without grazers. For

222 grasses, the continuous consumption by grazers removes aboveground biomass at a higher

223 rate than by normal senescence in the simulation without grazers. For the total vegetation as a

224 whole, turnover rate increased by 31%, not only because of faster cycling in grass and tree

225 biomass, but also because of the smaller total forest area (30 vs. 33 Mkm^2). More details on

226 the effect of grazing on tree cover and carbon stocks and fluxes can be found in
227 Supplementary Discussion.

228 **Discussion**

229 We implemented dynamic herbivores and their effects on vegetation types and the land
230 carbon cycle in the ORCHIDEE-MICT DGVM model, based on physiological and
231 demographic equations for large grazers. Evaluation against today's empirical herbivore
232 biomass data for protected areas across a wide range of ecosystems shows a reasonable model
233 performance in simulating potential grazer biomass sustained by the grassland ecosystems.
234 We then presented the global results of potential large grazer biomass for present-day and the
235 LGM.

236 In the context of the so-called productivity paradox of the late Pleistocene mammoth steppe
237 biome, our model shows that only if the prescribed average body size was much higher than
238 today (500 vs. 180 kg ind.$^{-1}$) could high grazer densities be simulated under the harsh climate
239 and low atmospheric CO_2 during the LGM. This property emerges from the different scaling
240 of forage intake and energy expenditure with body size, namely, the allometric exponent of
241 intake (0.88 for living grass and 0.84 for dead grass, Methods equation (1)) is higher than the
242 exponent of expenditure (0.75, Methods equation (3)), the former from an animal model
243 calibrated for cattle[34], and the latter conforming to the metabolic theory[48]. A collection of
244 body mass and dry matter intake across 46 large mammalian herbivores (body weight > 10
245 kg)[49] gives a value of 0.85 for the scaling exponent (Supplementary Fig. 7), which is indeed
246 higher than the 3/4 power scaling of metabolic rates and production rates[37,50], and supports the
247 high values used in our model. Note that the exponent of intake increases with forage
248 digestibility (equation (1)), which are fixed values in the current model. In reality,
249 digestibility varies at different phase of growth, with higher values in the early growing
250 season, and decreases with the accumulating grass biomass[51]. Therefore, a potential positive
251 feedback of large grazers on forage digestibility is missing in the model. Besides, the scaling
252 exponent was reported to be different between ruminants (ca. 0.88) and hindgut fermenters
253 (ca. 0.82)[52], thus the value for an "average grazer" may be lower than the values used in the
254 current model, close to the regression coefficient of 0.85 by ref.[49].

255 Evidences from fossil[53,54] and extant[55] mammal species have shown a long-term trend towards
256 increasing body size in mammals throughout the Cenozoic, i.e. Cope's rule in evolutionary
257 biology[53]. This indicates selective advantages of larger body sizes, such as larger guts of

258   herbivores that allow microbes to break down low-quality plant materials, and higher

259   tolerance to coldness and starvation[55]. Our results show quantitatively the importance of body

260   size to explain the productivity paradox, as a larger-body size enables grazers to live on the

261   mammoth steppe in substantial densities during the LGM, despite colder temperatures and

262   shorter growing seasons than today. After the end-Pleistocene extinction of large-body size

263   species, to which the contributions of humans versus fast climate change remaining debated[56],

264   the average body size of herbivores reduces, and the boreal and arctic grasslands today can

265   only sustain a low biomass density of grazers (Figs. 2 and 4).

266   One limitation of our current model is a lack of separation among large herbivore species or

267   types, in particular a specific representation of megaherbivores (body mass > 1000 kg). The

268   keystone herbivore hypothesis is centred on the pivotal role of megaherbivores in creating and

269   maintaining an open habitat dominated by fast-growing, more nutritious short grasses and

270   woody plants, the habitat that is crucial for many smaller herbivores[24]. This appears to be

271   supported by observations in present-day Africa[57,58] that white rhino, not the smaller grazers,

272   were able to maintain short grass communities, the loss of which led to declines in smaller

273   grazers like impala and zebra. This interaction among plants, megaherbivores and smaller

274   ones is, however, dependent on vegetation productivity along environmental gradients[57,59].

275   Therefore, to expand the "average grazer" in our current model to a framework of herbivore

276   functional types (HFTs, e.g. refs[31,60]) is a future priority; and a mechanistically coupled HFTs

277   and vegetation dynamics in DGVM models could be a promising tool to quantitatively

278   investigate the ecological impacts of large herbivores.

279   For the ecological impacts of large grazers, our results show a general reduction of tree cover

280   and an increase in grassland productivity with grazers (Fig. 5 and Supplementary Discussion).

281   The current model, however, does not represent the composition changes of herbaceous

282   species under grazing (which favours annual over perennial plants, short over tall plants, and

283   high over low specific leaf area)[5,6], as well as competition between shrubs, mosses and

284   grasses under grazing pressure[4,61]. In a tundra ecosystem[61], a heavy grazing has led to a

285   transition from moss-rich heathland into graminoid-dominated steppe-like vegetation, and

286   thus increased the aboveground primary production. Therefore, to better simulate the grazer-

287   induced changes in biogeochemical cycle in DGVM models would require an explicit

288   representation of mosses and shrubs, and their competition with grasses affected by grazers. It

289   is worth noting that to disentangle the relative contribution of the factors, including species

290 changes and increased nutrient availability, to the enhanced productivity is difficult in field
291 grazer-exclusion experiments. The lack of a fully closed nutrient cycle in our model also
292 limits its accuracy to estimate the full impact of grazers on ecosystems.

293 What adds more complexity to the ecological impacts of large grazers is a set of physical
294 properties that are affected by grazing, especially in cold regions. As argued in refs[18,19,62],
295 during summer, by removing the insulating moss carpet and litter layer, large grazers might
296 increase soil temperature and deepen annual thaw depth and root penetration; during winter,
297 by trampling snow in search for food, they might lower soil temperature in winter, meanwhile,
298 quicken the spring melt of snow due to a lower albedo of dirty snow, and lengthen growing
299 season. To test the magnitude of such effects requires parameterization of these biotic-abiotic
300 interactions in future model developments. Large herbivores might have fundamentally
301 modified Pleistocene ecosystems; to bring them into large-scale land surface models would
302 help us better understand the intricate interactions among climate, plants and animals that
303 shaped the biosphere.
304

305 **Acknowledgements**

308

309 **Author contributions**

310 D.Z. and P.C. designed the study. D.Z. led the writing and performed the analysis, with
311 critical input from P.C. and G.K. J.C. contributed to the model development. S.P., N.V., J.P.
312 and S.Z. enriched the discussion of the results.

313

314 **Correspondence and requests for materials** should be addressed to D.Z.

315

316 **Competing interests**

317 The authors declare no competing financial interests.
318

319 **Methods**

320 **ORCHIDEE-MICT model overview**

321 ORCHIDEE (Organizing Carbon and Hydrology In Dynamic Ecosystems) is a process-based
322 DGVM model designed for multi-scale applications[32]. It consists of two main modules:
323 SECHIBA for energy and water exchanges and photosynthesis at half-hourly time-step, and
324 STOMATE for vegetation dynamics and carbon cycle at daily time-step (Fig. 1). The model
325 describes the land surface using a "tile" approach, i.e. each grid cell is occupied by a set of
326 plant functional types (PFTs), with the fractional covers of all PFTs adding up to one. In the
327 current model there are 13 PFTs, including 8 for trees, 2 for natural grasses (C3 and C4), 2 for
328 crops, and bare land. PFTs go through the same suite of processes (photosynthesis, phenology,
329 allocation of carbon assimilates to plant biomass compartments, carbon flow from living
330 biomass to litter pools after senescence and/or mortality, and from litter to soil carbon pools,
331 and heterotrophic respiration), but with PFT-specific parameter values, as detailed in ref[32].
332 Vegetation distribution, i.e. fractional covers of the PFTs, is simulated by the vegetation
333 dynamics module through bioclimatic limits, competition between PFTs for space and light,
334 and a series of mortality process[33]. The soil thermal and hydrological dynamics are
335 represented by a physically based multi-layer soil structure to simulate heat transfer and water
336 movement between air and deeper soils[63,64]. These physical processes interact with the
337 vegetation and carbon processes mentioned above (Fig. 1).

338 Inputs required by ORCHIDEE include meteorological variables (surface air temperature,
339 precipitation, air humidity, incoming short and long wave radiation, wind, and air pressure),
340 atmospheric CO_2 concentration, and soil texture. For each simulation, the model needs to run
341 at first a period of "spin-up", namely, starting from zero carbon fluxes and pools, full cover of
342 bare land, and default values for physical variables, the model gradually approaches an
343 equilibrium state given the inputted climate and atmospheric CO_2 conditions. Then, transient
344 simulations for the target time period can be conducted from the last year of spin-up. In
345 ORCHIDEE, the spatial resolution of each simulation depends on the resolution of input
346 climate forcing.

347 ORCHIDEE-MICT is an evolution of ORCHIDEE with additional high latitude processes,
348 including a soil freezing scheme which simulates the liquid and solid water fractions in the
349 soil and associated energy balance[65], a multi-layer snow scheme which improves the
350 representation of snow thermal conductivity and soil temperature[66], and a vertically resolved
351 litter and soil carbon module considering permafrost processes[67,68].

352 To incorporate grazing processes in ORCHIDEE-MICT, we firstly adapted the structure of
353 the ORCHIDEE-GM version 2.1 (grassland management, ref[69]), originally designed to
354 simulate the greenhouse gas balance of pastures, including forage consumption by grazing
355 that decreases aboveground living biomass and keeps leaf age younger, excreta return that
356 affects the decomposability of the litter pools, and animal respiration. We also revised two
357 photosynthesis parameters for the grass PFTs, namely the maximum rate of Rubisco

358 carboxylation (v_{cmax}) and the maximum specific leaf area (SLA_{max}), to be the same as those
359 calibrated by Chang et al.[70] based on literature analysis for modern grasslands. As in
360 ORCHIDEE-GM, we simulate large grazers only, so biomass intake through browsing on
361 woody plants is not included. The carbon mass simulated by ORCHIDEE-MICT is converted
362 into dry matter mass used in the grazing module by dividing by 0.45. We further adapted the
363 grazer population model of Illius and O'Connor[34] into ORCHIDEE-MICT, which calculates
364 energy intake and expenditure, reproduction, and mortality using empirical relationships with
365 body size. A major difference from the original equations proposed by Illius and O'Connor
366 model is that we did not separate animals into age classes, thus there is only one type of
367 "average grazer" with fixed mature body mass (denoted as A). Detailed implementations are
368 described below.

The grazer population model

Daily intake and expenditure

371 For wild large grazers, the reduction in food resources during the non-growing season
372 critically limits their density[71]. Unlike domestic livestock on pastures that can be fed on
373 forage grass or crop products, wild herbivores resort to various ways to acquire energy during
374 the non-growing season, such as migration and feeding on dead grasses[72]. In the grazing
375 module in ORCHIDEE-MICT, in order to sustain grazers throughout the year, especially for
376 the high latitude regions with a short growing season, we divided the simulated aboveground
377 litter pool of grass PFTs into two parts, an edible pool (L_{edi}, representing plant residues) and
378 an inedible one (representing animal excreta) (Fig. 1). Grazers are allowed to eat L_{edi} when
379 confronted with insufficient AGB (aboveground grass biomass of three tissues represented in
380 ORCHIDEE, i.e. leaf, sapwood and fruit).

381 **Maximum daily intake.** The maximum forage intake in units of energy is related to grazers'
382 body size and forage digestibility (d), since a low digestibility diet decreases the rate of
383 digestion of ungulates and thus limits the maximum intake[52,73], which is calculated as in Illius
384 and O'Connor model[34]:

385
$$I_{max} = 0.034e^{3.57d} A^{(0.077e^d +0.73)} \tag{1}$$

386 where I_{max} (MJ d^{-1} ind.$^{-1}$) is the maximum daily net energy intake per individual; A (kg live
387 weight ind.$^{-1}$) the mean grazer body mass; d the forage digestibility, fixed at 0.7 for AGB and
388 0.4 for L_{edi}, following ref[34].

389 The maximum intake in units of dry mass is converted from I_{max} by:

390
$$I_{DM,max} = \frac{I_{max}}{ME \times DE} \tag{2}$$

391 where $I_{DM,max}$ (kgDM d^{-1} ind.$^{-1}$) is the maximum daily dry matter intake; ME (MJ kgDM^{-1}) the
392 metabolizable energy content, calculated as 15.6×d, following Pachzelt et al.[30]; DE the
393 digestible energy proportion in the forage not excreted in the faeces, fixed as 50%[74].

394 **Daily energy expenditure.** Energy expenditure in the original Illius and O'Connor model[34]
395 applied to tropical grasslands was a function of body mass only, and did not account for

13

396 environmental conditions. Ambient temperature has been shown to significantly affect energy
397 expenditure for endotherms[50]. Since we aim to apply the model globally, we introduce the
398 following equation to account for temperature dependent metabolic rate:

399 $$E = \frac{k_2}{e^{k_1 \times T}} \times A^{0.75} \tag{3}$$

400 where E (MJ d^{-1} ind.$^{-1}$) is the daily energy expenditure per individual; T (°C) the long-term
401 mean air temperature for each grid cell, calculated in the model using a linear relaxation
402 method (see Eq. 3 in Krinner et al.[32]) with the integration time equaling to 3 years; k_1 equals
403 to 0.0079, derived from the regression model of Anderson and Jetz[50]; k_2 equals to 0.36,
404 calibrated to yield a range close to the values in ref[34]. Note that this parameterization may
405 overestimate energy expenditure for the large herbivores adapted to cold climates like woolly
406 mammoth and muskox, which may spend less energy due to the insulating heavy hair coat
407 and thick fat layer[26].

408 **Conversion between energy and fat storage.** Fat is the main energy reserve and affects the
409 survival of grazers confronted with food shortages[73]. The daily change in fat storage is
410 calculated as:

411 $$\frac{dF}{dt} = \frac{I - E}{m} \tag{4}$$

412 where F (kg ind.$^{-1}$) is the fat mass per animal; I (MJ d^{-1} ind.$^{-1}$) the actual daily net energy
413 intake (described below); m (MJ kg^{-1}) the conversion coefficient between energy and fat, set
414 at 39.3 if $I<E$ (catabolism) or 54.6 if $I>E$ (anabolism) (ref[34]). Note that the body mass, A, is a
415 fixed parameter in the model, neglecting the daily-changing F.

416 **Actual daily intake.** Actual daily intake depends on the amount of available forage. At each
417 daily time step, the model determines whether grazers feed on AGB, L_{edi}, or nothing, by
418 comparing the daily forage requirement, calculated as $I_{DM,max} \times P$, given a population density P
419 (ind. km^{-2}) calculated by the model (see below), with the amount of available AGB or L_{edi}.
420 Grazers are assumed to feed in priority on i) AGB, if available AGB exceeds the AGB
421 requirement; ii) L_{edi}, if condition i) is not met and L_{edi} exceeds the L_{edi} requirement; and iii)
422 nothing, if neither conditions i) nor ii) are met. Note that $I_{DM,max}$ for AGB is higher than for
423 L_{edi}, i.e. the AGB requirement is always higher than the L_{edi} requirement, according to
424 equation (1) and (2). A buffer time of five days is set to prevent grass from being grazed at the
425 beginning of the growing season, i.e. the grazers are assumed to wait for five days to eat AGB
426 after it first exceeds the forage requirement.

427 Actual intake also has a constraint so that a maximum fat storage cannot be exceeded, which
428 is given by:

429 $$I = \begin{cases} I_{\max} & if \quad F + \dfrac{I-E}{m} \leq F_{\max} \\ m \times (F_{\max} - F) + E & else \end{cases} \tag{5}$$

430 where F_{max} (kg ind.$^{-1}$) is the maximum fat mass, set at $0.3 \times A$ (ref[34]).

431 Note that the reduction factor of $I_{\max}$ with decreasing vegetation biomass density in the
432 original Illius and O'Connor model[34] is not used here, assuming that the grazers have good

14

433 access to the forage and can fulfil their daily demand whenever *AGB* or L_{edi} is higher than the
434 forage requirement.

435

Grazer population dynamics

437 In ORCHIDEE-MICT, the grazer population density is updated at the end of each year, based
438 on calculated annual mean birth and mortality rates, as described in the following.

439 **Birth rate.** Birth rate depends on body condition, represented by a function of the ratio of the
440 fat storage to the maximum fat mass, following ref[34]:

$$441 \quad B_{max} = \frac{0.8}{1 + e^{-15 \times (\frac{F}{F_{max}} - 0.3)}} \tag{6}$$

442 where B_{max} (yr^{-1}) is the maximum birth rate, calculated at daily time-step and averaged over
443 the year to be used in equation (7).

444 In this study, the actual birth rate is also constrained by fat storage, which implicitly considers
445 the energy investment in breeding:

$$446 \quad B = Minimum(B_{max}, \frac{m \times F}{E \times 365}) \tag{7}$$

447 where B (yr^{-1}) is the actual birth rate at the end of the year. Then the amount of energy
448 $\frac{B \times E \times 365}{m}$ is subtracted from F to account for the energy transferred to newly added grazers.

449

450 **Mortality rate.** In the Illius and O'Connor model[34], mortality was caused by the exhaustion
451 of fat storage during periods of food shortage. In ORCHIDEE-MICT, we define it as
452 starvation-induced mortality (M_s), and calculate it using the same method as in Illius and
453 O'Connor model: we assume the fat storage to be a normal distribution with a mean
454 $\mu = F$ and a standard deviation $\sigma = 0.125 \times F_{max}$; then the cumulative distribution function of
455 fat storage returns the probability (defining the value for M_s) that fat mass is below a
456 prescribed threshold F_{thresh}. The value of F_{thresh} was set at 0 in the original Illius and
457 O'Connor model, but we set F_{thresh} at $-0.2 \times F_{max}$, so that the grazers, especially those on
458 temperate and boreal grasslands, could tolerate longer periods of starvation. The mortality rate
459 M_s in the unit of yr^{-1} is calculated at daily time-step and averaged over the year.

460 In addition to M_s, two other causes of mortality are taken into account: i) a background
461 mortality rate (M_b) which is defined as the inverse of animal lifespan, fixed at 25 years[30]; and
462 ii) a density-dependent mortality rate ($M_d=k_d \times P$) which represents the fact that a higher
463 density leads to a more intensive competition between animals for limited resources (e.g.
464 water and living space), and to more frequent epizootic diseases.

465 Therefore, the equation to calculate the dynamic annual evolution of grazer population density
466 is:

$$467 \quad \frac{dP}{dt} = B \times P - M_b \times P - M_s \times P - k_d \times P^2 \tag{8}$$

468 where P (ind. km^{-2}) is the grazer population density, updated each year; P is initialized as

15

469 P_0=0.001 ind. km^{-2}; whenever P is below P_0, P is reset to P_0 and F is reset to 0; k_d is the slope
470 of the density-dependent mortality function, calibrated based on the property of equation (8)

471 that the maximum P equals to $\dfrac{B-M_b}{k_d}$ given an infinite time under constant optimal condition

472 (M_s =0, M_b =0.04, and $B \approx 0.6$ according to Eqs. 6 and 7); the value of k_d is therefore set at

473 $\dfrac{A}{3\times10^4}$, derived from observed maximum densities of 15~18×10^3 kg km^{-2} for large herbivore

474 biomass observed in protected areas across Africa today (Hatton et al.[37]; Supplementary Table
475 1).

Effects of grazers on vegetation

477 A direct negative impact of grazers on grass productivity is through biomass removal by
478 grazing. This is included in the coupling between grazing and carbon cycle processes, as leaf
479 area index (LAI) is updated every day in the model following the leaf mass reduction. Besides,
480 a positive effect on grass productivity due to regrowth after defoliation is represented in the
481 model by, first, the leaf age-related photosynthetic capacities, with younger leaves having a
482 higher photosynthetic efficiency (see Eq. A12 in Krinner et al.[32]), and second, the leaf age-
483 related specific leaf area (SLA), with younger leaves having a higher SLA and subsequently a
484 more rapid increase in LAI after a daily grazing event than if SLA was constant[69]. Grazers
485 could also positively affect grass productivity through accelerating nutrient turnover and
486 modifying the traits and composition of herbaceous species[7,10,61], which may be more
487 important than the regrowth effect. To explicitly represent these effects is difficult, partly
488 because that our model lacks an explicit nutrient cycle and has limited herbaceous plant
489 functional types (only two grass PFTs, C3 and C4, for natural non-woody plants) with fixed
490 sets of traits, partly because that the observed enhancement of grass production by grazing in
491 field experiments is a result of various effects mentioned above, making it difficult to be used
492 for calibrating parameters for each individual pathway in a model. Therefore, we used a
493 simple parameterization, i.e. a grazer density-related photosynthetic capacity, to coarsely
494 approximate the positive effects of grazers associated with accelerated nutrient cycling and
495 traits/composition changes, as detailed below.

496

Grazer density-related v_{cmax} and j_{max}

498 The enhancement of primary production by grazing has been observed in a wide range of
499 ecosystems, such as African savannahs[75,76], North American grasslands[9], and Arctic tundra[8,61],
500 but few studies have reported measurements of both grazer density and its quantitative effect
501 on grass productivity. A field study by Frank and McNaughton[9,77] in Yellowstone national
502 park found a 11-85% higher aboveground net primary production (ANPP) for grazed than
503 ungrazed vegetation, with 23-90% of the ANPP consumed by herds of elk and bison, from
504 which a herbivore density of 2-18×10^3 kg km^{-2} was inferred.

505   We thus made a simple modification to the photosynthesis parameters of the maximum rate of
506   Rubisco carboxylation (v_{cmax}) and electron transport (j_{max}) (the latter is dependent on v_{cmax} in
507   the model) for the grass PFTs as a function of grazer density:

508    $$v_{cmax} = v_{cmax}^0 \times [1 + (k_a - e^{-k_b \times A \times P})] \tag{9}$$

509   where k_a equals to 1, i.e. a maximum 2-fold increase from animal-induced nutrient availability,
510   qualitatively in agreement with the results of grassland fertilization experiments compiled by
511   Elser et al.[78] giving a response ratio of 1.7~2 (primary production in grassland manipulative
512   experiments with nitrogen and phosphorus addition divided by the value in control
513   treatments). The parameter k_b is set at 10^{-4}, calibrated based on the observed response of
514   ANPP to herbivores by Frank and McNaughton[9,77] cited above.

515

Tree mortality caused by large grazers

517   The suppression of trees and shrubs by large mammalian herbivores, favouring grass species,
518   has been observed in African national parks[79,80] and Arctic tundra[4,81]. In their tree-population
519   dynamics model developed for the Serengeti-Mara woodlands, Dublin et al.[82] proposed a tree
520   mortality caused by elephants of 7% yr^{-1} when the elephant biomass density was ca. 2000 kg
521   km^{-2}, which accounted for 25% of the total herbivore biomass in that region[37]. This grazer-
522   induced tree mortality is higher than the simulated tree mortality in tropical forests by
523   ORCHIDEE-MICT[33] of about 3% yr^{-1}.

524   Since the current version of ORCHIDEE-MICT lacks a specific shrub PFT, we introduced a
525   grazer trampling-related mortality only for the tree PFTs, defined as a linear function of
526   grazer population density:

527    $$M_{tree,tramp} = k_{tree,tramp} \times A \times P \tag{10}$$

528   where $M_{tree,tramp}$ is the grazing-induced mortality rate of tree PFTs each day (d^{-1}); $k_{tree,tramp}$ is
529   set at 2.4×10^{-8} d^{-1}, in order to match the observed elephant-induced tree mortality in
530   Serengeti-Mara[82].

Evaluation data

Empirical present-day herbivore data

533   To evaluate the model, we compared the simulated present-day grazer density with the
534   empirical data for large wild mammalian herbivores across various ecosystems (with low
535   human footprints) compiled by Hatton et al.[37]. Since Hatton et al.[37] focused on predator-prey
536   relationships and excluded megaherbivores like elephant and rhinoceros, we re-calculated the
537   total herbivore biomass density of each community, including all reported herbivore species
538   from the raw data provided by Hatton et al.[37]. Multi-year data for the same ecosystem were
539   averaged, giving 23 protected areas in Africa, 25 in Asia, and 15 ecosystems in North
540   America (Supplementary Table 1). Note that the 15 ecosystems in North America are not
541   game reserves, and human hunting probably decreases animal densities below the local
542   carrying capacities. The empirical herbivore biomass data in Hatton et al.[37] included both
543   grazers and browsers, while our model could only simulate grazer densities. In the model-data

544 comparison, it was thus assumed that grazers dominated the herbivore species[30], which may
545 be ecosystem-specific.

546

Reconstruction data for paleo-megafauna

548 Few studies have investigated the megafaunal populations and biomass densities in the
549 mammoth steppe during the late Pleistocene. By analysing ^{14}C-dated animal bones
550 accumulated in frozen loess in Siberia and Alaska, Zimov et al.[19] estimated an average
551 herbivore biomass of 10 tonne km^{-2} over the period of 40-10 ka BP in northern Siberia, and
552 Mann et al.[23] estimated a similar value of 9 tonne km^{-2} for the same period in arctic Alaska.
553 Although the bone abundance varies markedly with time, suggesting temporal instability of
554 the mammoth steppe during the 30,000-year period[45], these estimates are the best available to
555 date providing information on the magnitude of the biomass of large herbivores at the LGM
556 for comparisons with the simulations.

557 The geographical ranges of ice-age megafaunal species are useful indicators of their presence
558 in a grid-point of the model. Lorenzen et al.[22] compiled a dataset of ca. 800 dated megafaunal
559 fossil localities spanning the past 50,000 years. As a compromise between the number of
560 localities and the period that could be considered coeval to the LGM, we selected the time
561 interval of 26.5-20 ka BP[83] of these fossil localities (in total 215 localities) to compare with
562 our results at the LGM. Note that debate still exists in the chronological definition of LGM
563 (e.g. ref[84]), and that northern ice sheets peaked before 21 ka BP[83]. Overlaying the fossil
564 localities onto the simulated biomass density of large grazers enables a qualitative evaluation
565 of the model results, knowing that the incomplete list of fossil localities may under-represent
566 the megafauna's actual distribution ranges[22].

Model setup

568 Global runs with ORCHIDEE-MICT for present-day and LGM were conducted, as described
569 below and summarized in Table 1.

Present-day

571 For the present-day run (hereafter "PD"), ORCHIDEE-MICT was forced by the 6-hourly
572 CRU-NCEP gridded climate dataset at 2° spatial resolution
573 (https://vesg.ipsl.upmc.fr/thredds/fileServer/store/p529viov/cruncep/readme.html). The
574 model was first run for a 200-year spin-up to reach equilibrium for vegetation biomass and
575 grazers for the pre-industrial period (PI), forced by repeating the CRU-NCEP 1901-1910
576 climate data (due to lack of gridded climate data for PI) and constant pre-industrial CO_2
577 concentration (285 ppm). Then a transient simulation for 1860-2010 was started from the last
578 year of the spin-up, forced by CRU-NCEP reanalysis data from 1901 to 2010 (for 1860-1900,
579 CRU-NCEP 1901-1910 climate were cycled) and by rising CO_2 concentrations. The model
580 results for grazer biomass density averaged from 1960 to 2009 were used as PD, which
581 roughly corresponded with the period for the data compiled by Hatton et al.[37]. Since grazers

582   in the model only appear on the grass fraction of the land, grazer biomass density for the
583   entire grid cell was thus calculated using the following equation:

584    $$GB_i = P_{i,c3} \times A \times V_{i,c3} + P_{i,c4} \times A \times V_{i,c4} \qquad\qquad (11)$$

585   where GB_i (kg km^{-2}) is the grazer biomass density for grid cell i; $P_{i,c3}$ and $P_{i,c4}$ (ind. km^{-2}) are
586   the respective grazer population densities for the two types of grass PFTs, C3 and C4; and
587    $V_{i,c3}$ and $V_{i,c4}$ are the fractional cover of the two grass PFTs.

588   The grazer body size, A, is a key parameter in the model. Note that the value of A, in the
589   concept of "average grazer" in our current model, is the abundance-weighted average body
590   size over different species, i.e. total animal biomass divided by total animal population. For
591   PD, since ref[37] provided the population of each herbivore species, a mean body size of ca. 300
592   kg across 23 ecosystems in Africa and of ca. 180 kg across the ecosystems in both Asia and
593   North America was derived. Therefore, we prescribed A at 300 kg ind.$^{-1}$ for Africa and 180 kg
594   ind.$^{-1}$ for the rest of the world in the PD run.

595   Only natural PFTs were simulated in all runs, excluding agricultural land cover. So the results
596   represent a potential grazer biomass density without considering the replacement of wildlife
597   habitats by human land use. The PD results can be compared locally with observations from
598   Hatton et al.[37], which are from either protected areas or remote areas subject to minor human
599   effects. For the modelled global distribution as shown in Fig. 2a, the fractional covers of
600   tropical rainforest were subtracted from the direct output of potential grazer density (see
601   Supplementary Note 1). Then, in order to estimate the reduction of wild grazers due to human
602   land use, we applied the Anthromes version 2 map[41], which separated three major categories:
603   Used, Seminatural, and Wild (accounting for a total area of 71, 25, and 32 million km2
604   respectively for the year 2000), to subtract the fraction of the Used category (or Used +
605   Seminatural categories) in each 2° grid cell from the modelled potential grazer biomass, and
606   calculated the relative reductions regionally and globally (Supplementary Table 2).

607

608   **LGM**

609   For the LGM (21 ka BP) runs, the climate forcing files were the same as those described in
610   Zhu et al.[67], derived from the simulated LGM climate by the Earth System Model IPSL-
611   CM5A-LR, with a 6-hourly time-step and a spatial resolution of 1.875°×3.75°, bias corrected
612   using the differences between IPSL-CM5A-LR and observed climate in the historical period[67].
613   Atmospheric CO_2 for the LGM was fixed at 185 ppm[85], and the land-sea mask was prescribed
614   following the PMIP3 protocol (http://pmip3.lsce.ipsl.fr/). The model was run for 250 years;
615   the first 200 years were discarded as spin-up, and the last 50 years were averaged and
616   presented as the results.

617   For the LGM, the body size A was set at 500 kg ind.$^{-1}$, derived from the reconstructed
618   population density and biomass for several large herbivore species based on their relative
619   bone abundance by Mann et al.[23] and Zimov et al.[19]. We also tested the effect of body size by
620   carrying out a similar LGM run except for setting A at 180 kg ind.$^{-1}$, the same as that used in
621   the PD run for the northern hemisphere. To study the effects of grazing on vegetation, an

19

622 LGM run in which the grazing module was deactivated was conducted (denoted as "LGM-
623 noGrazer").

624
625 Table 1. Summary of the global runs with ORCHIDEE-MICT for present-day and LGM

	Spin-up		Transient simulation		Spatial resolution	Prescribed grazer body size (A, kg ind.[-1])
	Climate forcing	Atmospheric CO_2	Climate forcing	Atmospheric CO_2		
Present-day	CRU-NCEP 1901-1910 cycle	Pre-industrial level (285 ppm)	CRU-NCEP 1901-2010	Rising (ref[86] after 1959, ref[87] before 1959)	2°×2°	300 for Africa, 180 for the rest of the world
LGM	Outputs from IPSL-CM5A-LR, bias corrected	185 ppm[85]	Same as the spin-up		1.875°×3.75°	500
LGM (A=180)	The same as "LGM" except body size prescribed as 180 kg ind.[-1]					
LGM-noGrazer	The same as "LGM" except de-activating the grazing module					

626

Code availability

628 The grazing model used in this study is implemented in the ORCHIDEE-MICT global
629 dynamic vegetation model, with its runtime environment developed at Le Laboratoire des
630 Sciences du Climat et de l'Environnement (LSCE), France. The model, as well as the scripts
631 to derive the results presented in this study from the model outputs, are available from the
632 corresponding author upon request.

Data availability

634 The relevant model outputs (in NetCDF format) are deposited in the PANGAEA repository at
635 [doi]. The other data that support the findings of this study are available from the References
636 or from the corresponding author (dan.zhu@lsce.ipsl.fr) on reasonable request.
637

References

1. Ripple, W. J. *et al.* Collapse of the world's largest herbivores. *Sci. Adv.* **1,** e1400103–e1400103 (2015).

2. Sandom, C., Faurby, S., Sandel, B. & Svenning, J.-C. Global late Quaternary megafauna extinctions linked to humans, not climate change. *Proc. Biol. Sci.* **281,** 20133254 (2014).

3. Asner, G. P. *et al.* Large-scale impacts of herbivores on the structural diversity of African savannas. *Proc. Natl. Acad. Sci.* **106,** 4947–4952 (2009).

4. Olofsson, J. *et al.* Herbivores inhibit climate-driven shrub expansion on the tundra. *Glob. Chang. Biol.* **15,** 2681–2693 (2009).

5. Díaz, S., Noy-meir, I. & Cabido, M. Can grazing of herbaceous plants be predicted response from simple vegetative traits? *J. Appl. Ecol.* **38,** 497–508 (2001).

6. Díaz, S. *et al.* Plant trait responses to grazing ? a global synthesis. *Glob. Chang. Biol.* **13,** 313–341 (2007).

7. Frank, D. a., Groffman, P. M., Evans, R. D. & Tracy, B. F. Ungulate stimulation of nitrogen cycling and retention in Yellowstone Park grasslands. *Oecologia* **123,** 116–121 (2000).

8. Olofsson, J., Stark, S. & Oksanen, L. Reindeer in uence on ecosystem processes in the tundra. *Oikos* **2,** (2004).

9. Frank, D. A. & McNaughton, S. J. Evidence for the promotion of aboveground grassland production by native large herbivores in Yellowstone National Park. *Oecologia* **96,** 157–161 (1993).

10. Falk, J. M., Schmidt, N. M., Christensen, T. R. & Ström, L. Large herbivore grazing affects the vegetation structure and greenhouse gas balance in a high arctic mire. *Environ. Res. Lett.* **10,** 45001 (2015).

11. Sinclair, A. R. E. *et al.* Long-Term Ecosystem Dynamics in the Serengeti: Lessons for Conservation. *Conserv. Biol.* **21,** 580–590 (2007).

12. Gill, J. L. Ecological impacts of the late Quaternary megaherbivore extinctions. *New Phytol.* **201,** 1163–1169 (2014).

13. Gill, J. L., Williams, J. W., Jackson, S. T., Lininger, K. B. & Robinson, G. S. Pleistocene Megafaunal Collapse, Novel Plant Communities, and Enhanced Fire Regimes in North America. *Science (80-.).* **326,** 1100–1103 (2009).

14. Rule, S. *et al.* The Aftermath of Megafaunal Extinction: Ecosystem Transformation in Pleistocene Australia. *Science (80-.).* **335,** 1483–1486 (2012).

15. Sher, A. V., Kuzmina, S. A., Kuznetsova, T. V. & Sulerzhitsky, L. D. New insights into the Weichselian environment and climate of the East Siberian Arctic, derived from fossil insects, plants, and mammals. *Quat. Sci. Rev.* **24,** 533–569 (2005).

16. Guthrie, R. D. *Frozen Fauna of the Mammoth Steppe: The Story of Blue Babe.* (University of Chicago Press, Chicago, 1990).

678   17.   Guthrie, R. D. Origin and causes of the mammoth steppe: a story of cloud cover,
679   woolly mammal tooth pits, buckles, and inside-out Beringia. *Quat. Sci. Rev.* **20,** 549–
680   574 (2001).

681   18.   Zimov, S. A. *et al.* Steppe-Tundra Transition : A Herbivore-Driven Biome Shift at the
682   End of the Pleistocene. *Am. Nat.* **146,** 765–794 (1995).

683   19.   Zimov, S. A., Zimov, N. S., Tikhonov, A. N. & Iii, F. S. C. Mammoth steppe : a high-
684   productivity phenomenon. *Quat. Sci. Rev.* **57,** 26–45 (2012).

685   20.   Kahlke, R.-D. The maximum geographic extension of Late Pleistocene Mammuthus
686   primigenius (Proboscidea, Mammalia) and its limiting factors. *Quat. Int.* **379,** 147–154
687   (2015).

688   21.   Yurtsev, B. a. The Pleistocene 'Tundra-steppe' and the productivity paradox: The
689   landscape approach. *Quat. Sci. Rev.* **20,** 165–174 (2001).

690   22.   Lorenzen, E. D. *et al.* Species-specific responses of Late Quaternary megafauna to
691   climate and humans. *Nature* **479,** 359–364 (2011).

692   23.   Mann, D. H., Groves, P., Kunz, M. L., Reanier, R. E. & Gaglioti, B. V. Ice-age
693   megafauna in Arctic Alaska: extinction, invasion, survival. *Quat. Sci. Rev.* **70,** 91–108
694   (2013).

695   24.   Owen-Smith, N. Pleistocene extinctions: the pivotal role of megaherbivores.
696   *Paleobiology* **13,** 351–362 (1987).

697   25.   Putshkov, P. V. The impact of mammoths on their biome: clash of two paradigms.
698   *Deinsea* **9,** 365–379 (2003).

699   26.   Hopkins, D. M., Matthews, J. V & Schweger, C. E. *Paleoecology of Beringia.* (New
700   York: Academic Press, 1982).

701   27.   Redmann, R. E. in *Paleoecology of Beringia* 223–239 (Elsevier, 1982).
702   doi:10.1016/B978-0-12-355860-2.50024-7

703   28.   Gerhart, L. M. & Ward, J. K. Plant responses to low [CO2] of the past. *New Phytol.*
704   **188,** 674–695 (2010).

705   29.   Prentice, I. C. *et al.* Chapter 15 Dynamic Global Vegetation Modeling : Quantifying
706   Terrestrial Ecosystem Responses to Large-Scale Environmental Change. (2007).

707   30.   Pachzelt, A., Rammig, A., Higgins, S. & Hickler, T. Coupling a physiological grazer
708   population model with a generalized model for vegetation dynamics. *Ecol. Modell.*
709   **263,** 92–102 (2013).

710   31.   Pachzelt, A., Forrest, M., Rammig, A., Higgins, S. I. & Hickler, T. Potential impact of
711   large ungulate grazers on African vegetation, carbon storage and fire regimes. *Glob.*
712   *Ecol. Biogeogr.* **24,** 991–1002 (2015).

713   32.   Krinner, G. *et al.* A dynamic global vegetation model for studies of the coupled
714   atmosphere-biosphere system. *Global Biogeochem. Cycles* **19,** (2005).

715   33.   Zhu, D. *et al.* Improving the dynamics of Northern Hemisphere high-latitude
716   vegetation in the ORCHIDEE ecosystem model. *Geosci. Model Dev.* **8,** 2263–2283
717   (2015).

718   34.   Illius, A. W. & O'Connor, T. G. Resource heterogeneity and ungulate population
719   dynamics. *Oikos* **89,** 283–294 (2000).

720   35.   Willerslev, E. *et al.* Fifty thousand years of Arctic vegetation and megafaunal diet.
721   *Nature* **506,** 47–51 (2014).

722   36.   Kartzinel, T. R. *et al.* DNA metabarcoding illuminates dietary niche partitioning by
723   African large herbivores. *Proc. Natl. Acad. Sci.* **112,** 8019–8024 (2015).

724   37.   Hatton, I. A. *et al.* The predator-prey power law: Biomass scaling across terrestrial and
725   aquatic biomes. *Science (80-.).* **349,** aac6284-aac6284 (2015).

726   38.   Prins, H. & Douglas-Hamilton, I. Stability in a multi-species assemblage of in East
727   Africa large herbivores. *Oecologia* **83,** 392–400 (1990).

728   39.   Fuller, T. Population dynamics of wolves in north-central Minnesota. *Wildl. Monogr.*
729   (1989).

730   40.   Jung, M. *et al.* Global patterns of land-atmosphere fluxes of carbon dioxide, latent heat,
731   and sensible heat derived from eddy covariance, satellite, and meteorological
732   observations. *J. Geophys. Res.* **116,** G00J07 (2011).

733   41.   Ellis, E. C., Klein Goldewijk, K., Siebert, S., Lightman, D. & Ramankutty, N.
734   Anthropogenic transformation of the biomes, 1700 to 2000. *Glob. Ecol. Biogeogr.* **19,**
735   no-no (2010).

736   42.   Ripple, W. J. *et al.* Collapse of the world's largest herbivores. *Sci. Adv.* **1,** 1-e1400103
737   (2015).

738   43.   Harrison, S. P. & Prentice, C. I. Climate and CO2 controls on global vegetation
739   distribution at the last glacial maximum: analysis based on palaeovegetation data,
740   biome modelling and palaeoclimate simulations. *Glob. Chang. Biol.* **9,** 983–1004
741   (2003).

742   44.   Harrison, S. P. *et al.* Evaluation of CMIP5 palaeo-simulations to improve climate
743   projections. *Nat. Clim. Chang.* **5,** 735–743 (2015).

744   45.   Mann, D. H. *et al.* Life and extinction of megafauna in the ice-age Arctic. *Proc. Natl.*
745   *Acad. Sci.* 201516573 (2015). doi:10.1073/pnas.1516573112

746   46.   Barnes, R. F. W. & Lahm, S. . A. An Ecological Perspective on Human Densities in the
747   Central African Forest. *J. Appl. Ecol.* **34,** 245 (1997).

748   47.   Krausmann, F. *et al.* Global human appropriation of net primary production doubled in
749   the 20th century. *Proc. Natl. Acad. Sci. U. S. A.* **110,** 10324–9 (2013).

750   48.   Brown, J. H., Gillooly, J. F., Allen, A. P., Savage, V. M. & West, G. B. TOWARD A
751   METABOLIC THEORY OF ECOLOGY. *Ecology* **85,** 1771–1789 (2004).

752   49.   Clauss, M., Schwarm, A., Ortmann, S., Streich, W. J. & Hummel, J. A case of non-
753   scaling in mammalian physiology? Body size, digestive capacity, food intake, and
754   ingesta passage in mammalian herbivores. *Comp. Biochem. Physiol. Part A Mol.*
755   *Integr. Physiol.* **148,** 249–265 (2007).

756   50.   Anderson, K. J. & Jetz, W. The broad-scale ecology of energy expenditure of
757   endotherms. *Ecol. Lett.* **8,** 310–318 (2005).

758   51.   McNaughton, S. J. Ecology of a Grazing Ecosystem : The Serengeti Author (s): S . J .
759   McNaughton Published by : Ecological Society of America Stable URL :
760   http://www.jstor.org/stable/1942578 Your use of the JSTOR archive indicates your
761   acceptance of JSTOR 鈥s Terms and Co. **55,** 260–294 (2009).

762   52.   Illius, A. W. & Gordon, I. J. Modelling the nutritional ecology of ungulate herbivores:
763   evolution of body size and competitive interactions. *Oecologia* **89,** 428–434 (1992).

764   53.   Alroy, J. Cope's Rule and the Dynamics of Body Mass Evolution in North American
765   Fossil Mammals. *Science (80-.).* **280,** 731–734 (1998).

766   54.   Smith, F. a *et al.* The Evolution of Maximum Body Size of Terrestrial Mammals.
767   *Science (80-.).* **330,** 1216–1219 (2010).

768   55.   Baker, J., Meade, A., Pagel, M. & Venditti, C. Adaptive evolution toward larger size in
769   mammals. *Proc. Natl. Acad. Sci.* **112,** 5093–5098 (2015).

770   56.   Barnosky, A. D. Assessing the Causes of Late Pleistocene Extinctions on the
771   Continents. *Science (80-.).* **306,** 70–75 (2004).

772   57.   Waldram, M. S., Bond, W. J. & Stock, W. D. Ecological Engineering by a Mega-
773   Grazer: White Rhino Impacts on a South African Savanna. *Ecosystems* **11,** 101–112
774   (2008).

775   58.   Cromsigt, J. P. G. M. & te Beest, M. Restoration of a megaherbivore: Landscape-level
776   impacts of white rhinoceros in Kruger National Park, South Africa. *J. Ecol.* **102,** 566–
777   575 (2014).

778   59.   Pringle, R. M., Palmer, T. M., Goheen, J. R., McCauley, D. J. & Keesing, F. Ecological
779   Importance of Large Herbivores in the Ewaso Ecosystem. *Smithson. Contrib. to Zool.*
780   43–53 (2011). doi:10.5479/si.00810282.632.43

781   60.   Hempson, G. P., Archibald, S. & Bond, W. J. A continent-wide assessment of the form
782   and intensity of large mammal herbivory in Africa. *Science (80-.).* **350,** 1056–1061
783   (2015).

784   61.   Olofsson, J., Kitti, H., Rautiainen, P., Stark, S. & Oksanen, L. Effects of summer
785   grazing by reindeer on composition of vegetation, productivity and nitrogen cycling.
786   *Ecography (Cop.).* **24,** 13–24 (2001).

787   62.   Schweger, C. E., Matthews, J. V., Hopkins, D. M. & Young, S. B. in *Paleoecology of*
788   *Beringia* 425–444 (Elsevier, 1982). doi:10.1016/B978-0-12-355860-2.50037-5

789

790   **References in Methods**

791

792   63.   de Rosnay, P., Polcher, J., Bruen, M. & Laval, K. Impact of a physically based soil
793   water flow and soil-plant interaction representation for modeling large-scale land
794   surface processesart. no. 4118. *J. Geophys. Res. - Atmos. J. Geophys. Res.* **107,** 4118
795   (2002).

796   64.   Wang, F., Cheruy, F. & Dufresne, J.-L. The improvement of soil thermodynamics and
797   its effects on land surface meteorology in the IPSL climate model. *Geosci. Model Dev.*
798   **9,** 363–381 (2016).

799   65.   Gouttevin, I., Krinner, G., Ciais, P., Polcher, J. & Legout, C. Multi-scale validation of a
800   new soil freezing scheme for a land-surface model with physically-based hydrology.
801   *Cryosph.* **6,** 407–430 (2012).

802   66.   Wang, T. *et al.* Evaluation of an improved intermediate complexity snow scheme in the

803   ORCHIDEE land surface model. *J. Geophys. Res. Atmos.* **118,** 6064–6079 (2013).

804 67. Zhu, D. *et al.* Simulating soil organic carbon in yedoma deposits during the last glacial
805   maximum in a land surface model. *Geophys. Res. Lett.* 1–10 (2016).
806   doi:10.1002/2016GL068874

807 68. Koven, C. *et al.* On the formation of high-latitude soil carbon stocks: Effects of
808   cryoturbation and insulation by organic matter in a land surface model. *Geophys. Res.*
809   *Lett.* **36,** L21501 (2009).

810 69. Chang, J. F. *et al.* Incorporating grassland management in ORCHIDEE: model
811   description and evaluation at 11 eddy-covariance sites in Europe. *Geosci. Model Dev.*
812   **6,** 2165–2181 (2013).

813 70. Chang, J. *et al.* Combining livestock production information in a process-based
814   vegetation model to reconstruct the history of grassland management. *Biogeosciences*
815   **13,** 3757–3776 (2016).

816 71. Velichko, A. A. & Zelikson, E. M. Landscape, climate and mammoth food resources in
817   the East European Plain during the Late Paleolithic epoch. *Quat. Int.* **126–128,** 137–
818   151 (2005).

819 72. Bliss, L. C., Heal, O. W., Moore, J. J. & Programme, I. B. *Tundra Ecosystems: A*
820   *Comparative Analysis*. (CUP Archive, 1981).

821 73. Illius, A. & Gordon, I. Scaling up from functional response to numerical response in
822   vertebrate herbivores. *Herbiv. Between Plants Predators* (1999).

823 74. IPCC (2006) 2006 IPCC Guidelines for National Greenhouse Gas Inventories,
824   Prepared by the National Greenhouse Gas Inventories Programme (eds Eggleston HS,
825   Buendia L, Miwa K, Ngara T, Tanabe K). IGES, Japan.

826 75. McNaughton, S. J. Ecology of a grazing ecosystem; The Serengeti. *Ecol. Monogr.* **55,**
827   259–294 (1985).

828 76. McNaughton, S. J., Ruess, R. W. & Seagle, S. W. Large mammals and process
829   dynamics in African ecosystem. *Bioscience* **38,** 794–800 (1988).

830 77. Frank, D. A. & McNaughton, S. J. The Ecology of Plants, Large Mammalian
831   Herbivores, and Drought in Yellowstone National Park. *Ecology* **73,** 2043–2058
832   (1992).

833 78. Elser, J. J. *et al.* Global analysis of nitrogen and phosphorus limitation of primary
834   producers in freshwater, marine and terrestrial ecosystems. *Ecol. Lett.* **10,** 1135–1142
835   (2007).

836 79. Caughley, G. The elephant problem–an alternative hypothesis. *Afr. J. Ecol.* **14,** 265–
837   283 (1976).

838 80. Dublin, H. T. Decline of the Mara woodlands: the role of fire and elephants [Abstract].
839   **1986,** 534–535 (1995).

840 81. Väisänen, M. *et al.* Consequences of warming on tundra carbon balance determined by
841   reindeer grazing history. *Nat. Clim. Chang.* **4,** 384–388 (2014).

842 82. Dublin, H. T., Sinclair, A. R. E. & McGlade, J. Elephants and Fire as Causes of
843   Multiple Stable States in the Serengeti-Mara Woodlands. *J. Anim. Ecol.* **59,** 1147
844   (1990).

845   83.   Clark, P. U. *et al.* The Last Glacial Maximum. *Science (80-.).* **325,** 710–714 (2009).

846   84.   Hughes, P. D. & Gibbard, P. L. A stratigraphical basis for the Last Glacial Maximum
847   (LGM). *Quat. Int.* **383,** 174–185 (2015).

848   85.   Monnin, E. *et al.* Atmospheric CO2 Concentrations over the Last Glacial Termination.
849   *Science (80-.).* **291,** 112–114 (2001).

850   86.   NOAA's   Earth   System   Research   Laboratory
851   http://www.esrl.noaa.gov/gmd/ccgg/trends/.

852   87.   Joos, F. & Spahni, R. Rates of change in natural and anthropogenic radiative forcing
853   over the past 20,000 years. *Proc. Natl. Acad. Sci.* **105,** 1425–1430 (2008).

854

Figure Legends

Figure 1. Coupling between the ORCHIDEE-MICT dynamic vegetation model and the grazing module. The grazing module, incorporated in this study, simulates wild grazer density supported by grassland production, and feedbacks (blue and red arrows) of grazers on vegetation (see Methods). The black arrows represent carbon fluxes among grass, grazer and litter.

Figure 2 | Modelled potential large grazer biomass density for present-day (1960-2009 mean). **(a)** Potential density without consideration of human land use, after subtracting the fractions of tropical rainforest (see Supplementary Note 1). The black crosses in (a) symbolize the locations of the empirical data from Hatton et al.[37], shown in (b) and listed in Supplementary Table 1. **(b)** Comparison between empirical herbivore biomass[37] and modelled potential grazer biomass (Pearson correlation coefficient r=0.55, n=63, p<0.01). The dashed line represents the 1-1 line.

Figure 3 | Modelled LGM biome distribution and large grazer biomass density. **(a)** Simulated biome distribution at the LGM, converted from the modelled plant functional types (PFTs) properties using the algorithm described in Supplementary Note 2, in comparison with reconstructions based on pollen and plant macrofossil records compiled by the BIOME 6000 project **(b)**. **(c)** Simulated grazer biomass density at the LGM for Northern Hemisphere (north of 20°N). Blue circles on (c) indicate the dated megafauna fossil localities compiled by Lorenzen et al.[22], corresponding to the time interval of 26-20 ka BP.

Figure 4 | Relationship between modelled grazer biomass and grass NPP, affected by temperature and body size. **(a)** Relationships between log-transformed grass NPP, grazer biomass and rainfall in present-day (PD) Africa. Points represent median values for 10 mm rainfall bins and are shown with regression lines using linear function for grazer biomass-grass NPP relationship (green) and quadratic function for grass NPP-rainfall (blue) and grazer biomass-rainfall (red) relationships. The grey open circles represent wild herbivore biomass data compiled by ref[46] for 41 sites in Africa. A 2-D version of this figure is also shown in Supplementary Fig. 4. **(b,c)** Relationship between the grazer biomass-to-grass NPP ratio and mean annual temperature (MAT) for PD and LGM. Circles represent median values for 0.5 ºC MAT bins, with the size of each circle proportionate to the number of pixels in each bin. A indicates grazer body size (kg ind.$^{-1}$) prescribed in the model: for PD, 180 (except in Africa where A = 300) is used according to Hatton et al.[37]; for LGM, 500 is used according to reconstructions by Mann et al.[23] and Zimov et al.[19], and a sensitivity test with A=180 is conducted (see Methods).

Figure 5 | Modelled global carbon fluxes (red arrows, unit: Pg C yr^{-1}) among different reservoirs at the LGM. (a) De-activating the grazing module; **(b)** activating the grazing module. The black numbers give the standing stocks of different pools at equilibrium, including tree and grass living biomass, litter, and grazers.

902
903

a

120°W 60°W 0° 60°E 120°E

60°N
30°N
0°
30°S
60°S

Grazer biomass (10³ kg km⁻²)
0   0.5   1   2   3   4   5   6   7   8

b

○ Africa
○ Asia
○ North America

Modeled potential grazer biomass (kg km⁻²)

Empirical herbivore biomass (kg km⁻²)
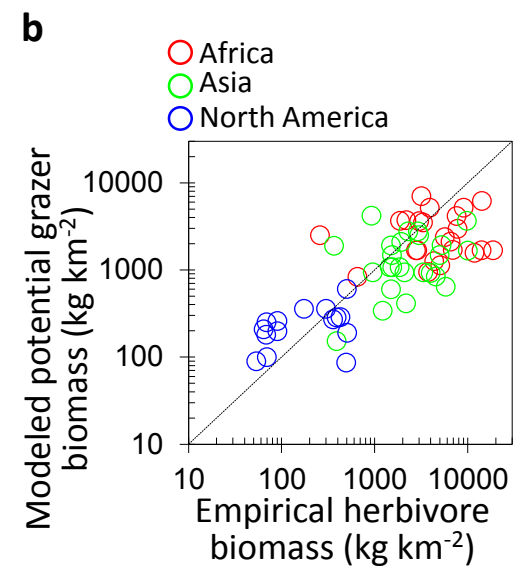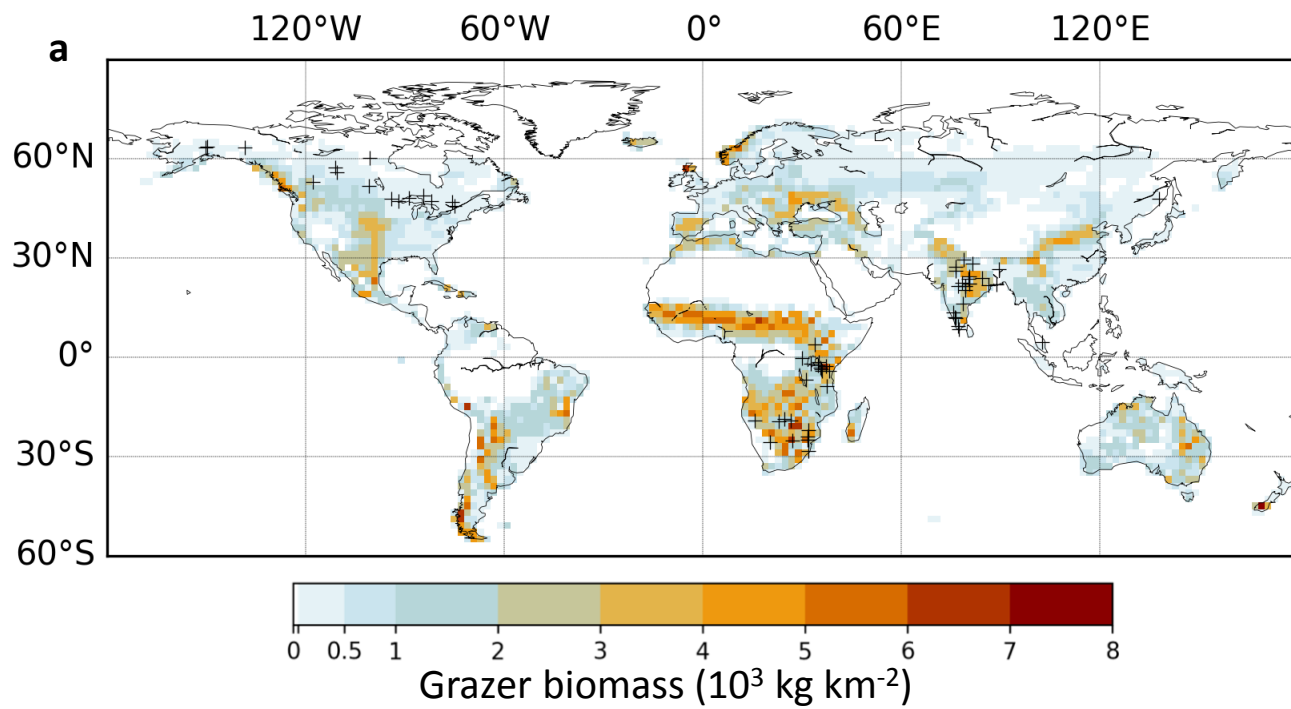
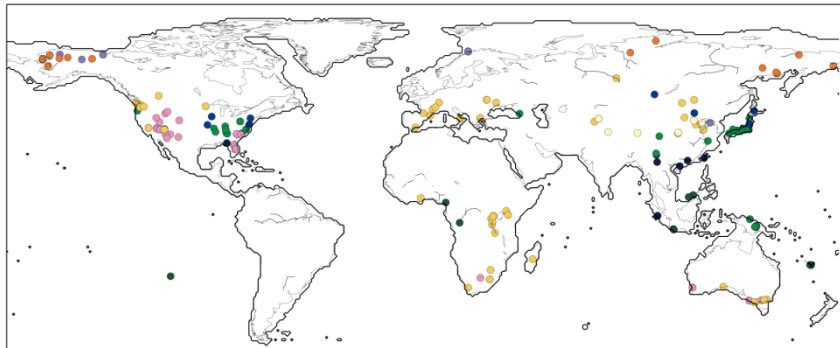**a** Modeled LGM biome distribution
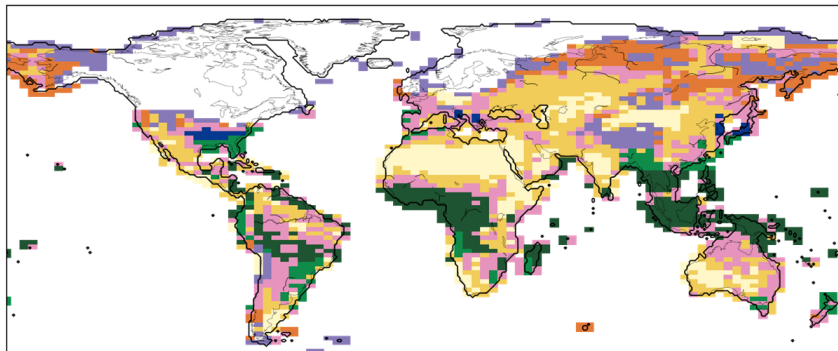
b Reconstructed LGM biome from BIOME 6000
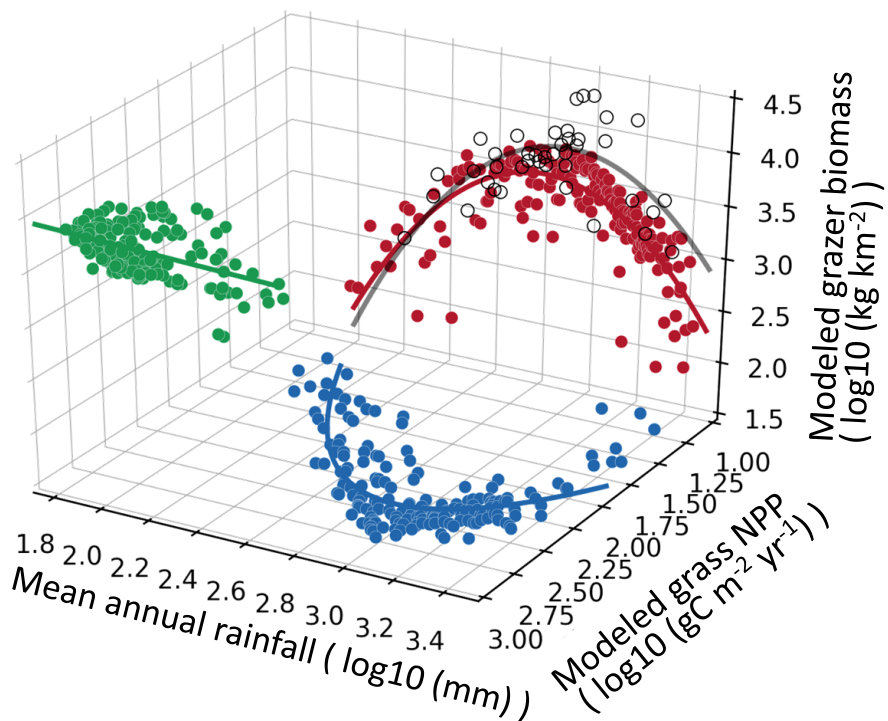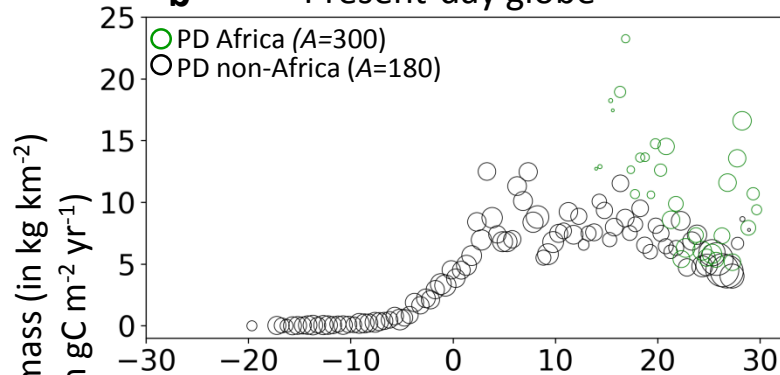
c Modeled LGM grazer biomass

Tropical forest | Warm-temperate forest | Savannah and dry woodland | Grassland and dry shrubland | Desert | Temperate forest | Boreal forest | Tundra | Dry tundra

Grazer biomass (10^3 kg km^{-2})
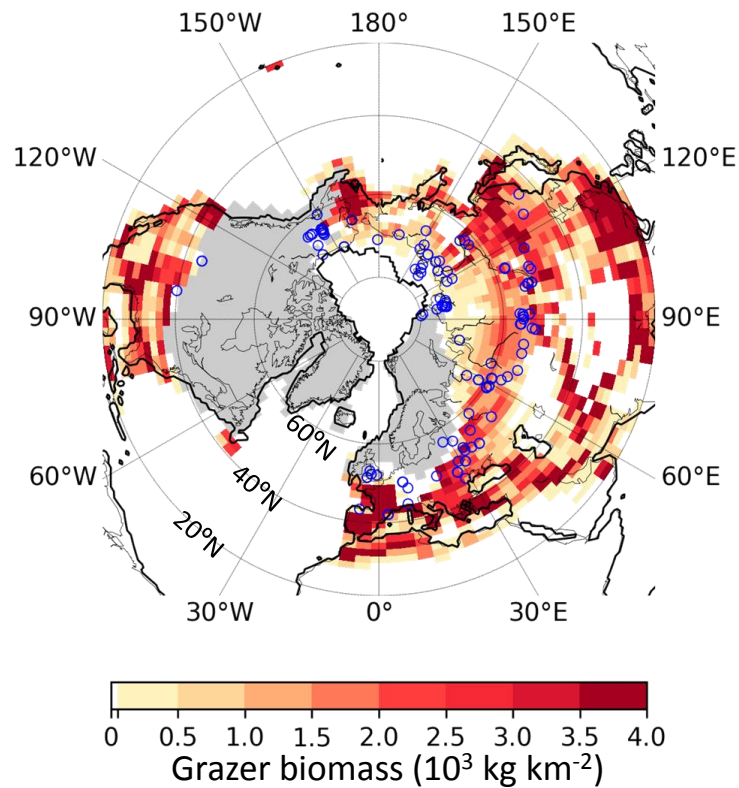
a Present-day Africa

b Present-day globe

c LGM globe

a

GPP (40) GPP (30)

tree (33 million km², 163 PgC)   grass (79 million km², 10 PgC)

Vegetation (173 PgC)

resp. (27)   resp. (13)

31

aboveground (65 PgC)

belowground (129 PgC)

Litter (194 PgC)

resp. (13)

14

Soil

LGM-noGrazer

b

resp. (0.9)

Grazers (319 million tonne live weight, or ca. 64 TgC)

GPP (37) GPP (40)   intake (1.5)   intake (0.2)   excreta (0.8)

tree (30 million km², 142 PgC)   grass (78 million km², 12 PgC)

Vegetation (154 PgC)

resp. (25)   resp. (17)

36

edible   inedible

aboveground (73 PgC)

belowground (140 PgC)

Litter (213 PgC)

resp. (15)

16

Soil

LGM-withGrazer